Article

Designing a New Framework Using Type-2 FLS and Cooperative-Competitive Genetic Algorithms for Road Detection from IKONOS Satellite Imagery

Maryam Nikfar [1,*], Mohammad Javad Valadan Zoej [1], Mehdi Mokhtarzade [1] and Mahdi Aliyari Shoorehdeli [2]

[1] Department of Photogrammetry and Remote Sensing, Faculty of Geodesy & Geomatics Engineering, K. N. Toosi University of Technology, Tehran 19967-15433, Iran; E-Mails: valadanzouj@kntu.ac.ir (M.J.V.Z.); m_mokhtarzade@kntu.ac.ir (M.M.)

[2] Control Department, Electrical Engineering Faculty, K. N. Toosi University of Technology, Tehran 19967–15433, Iran; E-Mail: m_aliyari@eetd.kntu.ac.ir

* Author to whom correspondence should be addressed; E-Mail: m.nikfar@mail.kntu.ac.ir; Tel.: +98-21-88877070 (ext. 328); Fax: +98-21-878-6213.

Abstract: The growing availability of high-resolution satellite imagery provides an opportunity for identifying road objects. Most studies associated with road detection are scene-related and also based on the digital number of each pixel. Because images can provide more details (including color, size, shape, and texture), object-based processing is more advantageous. Therefore, in this paper, to handle the existing uncertainty of satellite image pixel values, using type-2 fuzzy set theory in combination with object-based image analysis is proposed. Because the main challenges of the type-2 fuzzy set are parameter tuning and extensive computations, a hybrid genetic algorithm (GA) consisting of Pittsburgh and cooperative-competitive learning schemes is proposed to address these problems. The most prominent feature of our research in this work is to establish a comprehensive object-based type-2 fuzzy logic system that enables us to detect roads in high-resolution satellite images with no training data. The validation assessment of road detection results using the proposed framework for independent images demonstrates the capability and efficiency of our method in identifying road objects. For more evaluation, a type-1 fuzzy logic system with the same structure as type-2 is tuned. Evaluations show that type-1 fuzzy logic system quality in training is very similar to that of the proposed type-2 fuzzy

framework. However, in general, its lower accuracy, as inferred by validation assessments, makes the type-1 fuzzy logic system significantly different from the proposed type-2.

1. Introduction

The increasing availability of very high resolution (VHR) satellite images provides an opportunity to identify urban objects. Roads, as one of the most important civil structures in various areas of management, such as urban planning, navigation, and traffic management, are subjects of great concern that need to be extracted automatically because human intervention is still required and is expensive and time-consuming. To date, various techniques have been reported in the literature for this purpose. Most of the reported techniques are primarily pixel-based and sometimes accompanied by textural information extracted from rectangular regions, in which structural and conceptual information is not properly exploited. To overcome the shortcomings of the pixel-based methods and to reduce the semantic gap, region-based algorithms have been developed [1–3]. Also in image processing, we usually encounter many uncertainties such as those caused by projecting 3D objects into a 2D image, uncertain boundaries, nonhomogeneous regions, poor and non-uniform lighting conditions, non-linearity of the imaging system and digitizing analog pictures. To reduce the effects of vagueness in road detection in satellite images, Type 1 fuzzy sets (T1 FSs) have been proposed in some of the literature. However, T1 FSs cannot completely model all the available uncertainties as their membership functions are crisp. On the other hand, Type-2 fuzzy sets (T2 FSs), thanks to their more flexible fuzzy membership functions, are much more promising in cases with high uncertainties [4].

Hence, in this paper, a new framework is proposed and designed for road detection from VHR satellite images that is based on object-based image analysis and a Type-2 fuzzy logic system (T2 FLS). Because the main challenges for the T2 FSs are parameter tuning and extensive computations, a hybrid Genetic Algorithm (GA) consisting of Pittsburgh and cooperative-competitive learning (CCL) schemes is proposed to address these problems. This method, as described in Section 4, is implemented in five main steps: segmenting images and generating object-based features, finding optimum features using the GA and K nearest-neighbor (GA-KNN) strategy, designing T2 FLS and its optimization by use of a hybrid GA, and ultimately, enhancing and generalizing validation. The paper is organized as follows: Section 2 briefly describes related works. Basic concepts of T2 FLS are reviewed in Section 3. Section 4 discusses the proposed framework. Implementation and a general evaluation of the results obtained are presented in Section 5. Finally, the conclusions are summarized in the last section of this paper.

2. Related work

Mena presented a review of nearly 250 references on road extraction [5]. Starting from seed points, linear feature extraction methods that were developed using active contour models, called snakes, were presented by Laptev *et al.* and Gruen *et al.* [6,7]. Doucette *et al.* presented an automated road centerline extraction method that exploits spectral content from high-resolution multi-spectral images [8]. The method is based on anti-parallel edge centerline extraction and self-organized road mapping. Zhang and Couloigner introduced a wavelet approach for road extraction from high-spatial-resolution remotely sensed imagery [9]. Valadanzoej and Mokhtarzadeh extracted roads using artificial neural networks that concentrated on evaluating different structures of neural networks, along with different measuring units and descriptors [10]. Peng *et al.* updated outdated road maps by incorporating generic and specific prior knowledge into a multi-scale phase field model [11]. Valero *et al.* detected road networks using directional mathematical morphology [12]. Movaghati *et al.* extracted roads using particle filtering (PF) and extended Kalman filtering (EKF). Starting from an initial point, the EKF module is responsible for tracing the median axis of a single road segment, whereas the PF module begins operating at road intersections [13]. A multi-stage strategy for automatically extracting roads from high-resolution multispectral satellite images based on salient features was introduced by Mirnalinee. This method incorporates the salient features of roads using a probabilistic support vector machine (P-SVM) and dominant singular measure (DSM) [14]. Shao *et al.* introduced a fast linear feature detector for road extraction. Only ridge line (or bright ribbon) extractions that are mostly roads in aerial and satellite images are considered in this paper [15]. Shi *et al.* proposed a method for extracting main road centerlines using path openings and closings as well as the support vector machine (SVM) classifier from images with a spatial resolution of 6 meters. In the proposed method, roads wider than four pixels are considered [16]. A method for accurate road centerline extraction from a classified image is proposed by Miao *et al.* [17]. Also, some new research based on SAR imagery and LIDAR system has been done in the last year [18–21]. To overcome the shortcomings of the pixel-based methods and to reduce the semantic gap, region-based algorithms have been developed [1–3]. Region-based classification is known to achieve better results than pixel-based classification in processing HSR images [22–24]. A considerable number of studies have compared object-based approaches with traditional pixel-based classification methods [25–29]. Many of these studies have found that object-based methods typically produce higher classification accuracies than pixel-based methods do. A new work is proposed by Huang and Zhang based on SVM and a multi-feature model at both pixel and object levels [30,31]. Zarinpanjeh *et al.* used object-based analysis for road map updates [32]. Additionally, Grote *et al.* developed a method for road network extraction using object-based analysis [33]. To reduce the effects of vagueness in road detection from satellite images, T1 FSs have been proposed in some literature. Agouris *et al.* used fuzzy logic for segmentation of an image. In this method, brighter pixels are considered more likely to be closer to real road pixels. Then, a template-matching algorithm is applied along the user-defined direction to locate the best road position [34]. A system for road extraction from IKONOS multispectral imagery based on fuzzy logic is proposed by Amini *et al.* [35]. Hinz and Wiedemann present an approach for self-diagnosis which is a part of an existing road extraction system. In their paper, fuzzy set theory is used as theoretical framework for knowledge representation for evaluation [36]. Bacher and Mayer extracted areas with

parallel edges and homogeneous areas between them as training data. After that, the training areas are used for a fuzzy multispectral classification [37,38]. Mohammadzadeh *et al.* proposed a fuzzy-based mean calculation method, which was optimized by a particle swarm optimization. It evaluated best mean values for road detection to improve the fuzzy cost function [39]. Singh and Garg proposed a weighted membership function-based fuzzy c-means with spatial constraints approach for automated road extraction. Initially, spatially fuzzy clustering is used to classify the satellite images. For removing non-road segments, four intermediate stages are used to extract the road information [40]. Possessing crisp membership functions, T1 FSs are not able to model these uncertainties directly. T2 FSs, on the other hand, show more prosperous performance as they provide adequately satisfactory results in capturing uncertainties [41]. Because GAs are well known and have been widely used as a powerful global search technique, a large number of publications explored the use of GAs for designing fuzzy systems, so-called GFSs [42]. Different GFSs have been proposed in the literature for designing both T1 and T2 fuzzy rule-based systems to avoid the necessity of linguistic knowledge from domain experts [43–49]. In the respective literature, four basic genetic learning approaches have been used for GFSs:

- The Pittsburgh approach, in which every chromosome of the population encodes an entire rule base and they compete with each other throughout the evolutionary process [50–52].
- The Michigan approach, in which each chromosome represents a single rule and the whole population forms the rule base [53].
- Iterative Rule Learning (IRL) approach, in which each chromosome is indicative of a single rule. Furthermore, implementing an iterative search process, a rule generation algorithm adds new fuzzy rules to the rule base, one at a time [54–57].
- The cooperative-competitive learning (CCL) approach, in which the chromosomes compete and cooperate simultaneously [58–61]. This can be understood in two opposite ways: the individuals could collaborate for the same purpose and thus construct the solution together, or they could compete against each other for the same resources. The use of CCL algorithms is recommended when the following issues arise: the search space is huge, the problem may be decomposed into subcomponents or different coding schemes are used [62].

In this paper, due to the large search space of T2 FLSs, an optimization method for FLS that is a hybrid GA consisting of a CCL approach and also containing a Pittsburgh approach is proposed. To ensure the compatibility of definitions, a brief review on basic concept of T2 FLS is presented in the section.

3. Type-2 Fuzzy Logic System (T2 FLS)

Recently, T2 FLSs have gained popularity in a wide range of applications due to their ability to handle higher degrees of uncertainty. The concept of a T2 FS was first introduced by Zadeh as an extension of the T1 FS [63]. A subsequent investigation of the properties of T2 FSs and higher types was performed by Mizumoto and Tanaka [64,65], and recently, Mendel and John introduced completely new terminology to distinguish between T1 and T2 FSs [4]. As mentioned in the field of image processing, we usually encounter many uncertainties. Possessing crisp membership functions, T1 FSs are not able to model these uncertainties directly. T2 FSs, on the other hand, show higher

performance as they provide adequately satisfactory results in capturing uncertainties [41]. A T2 FS set is characterized by fuzzy membership function; the membership grade for each element is a fuzzy set within the interval [0, 1] as shown in Figure 1. Such sets can be used *in situ*ations where there are uncertainties about the membership values [66]. Interval-valued T2 fuzzy is a special T2 fuzzy, where the upper and lower bounds of membership are crisp and the spread of membership distribution is ignored with the assumption that membership values between upper and lower values are uniformly distributed or scattered with a membership value of 1. As mentioned above, T2 membership function provides additional degrees of freedom in FLSs because their membership functions are themselves fuzzy, which can be very useful *in situ*ations with many uncertainties.
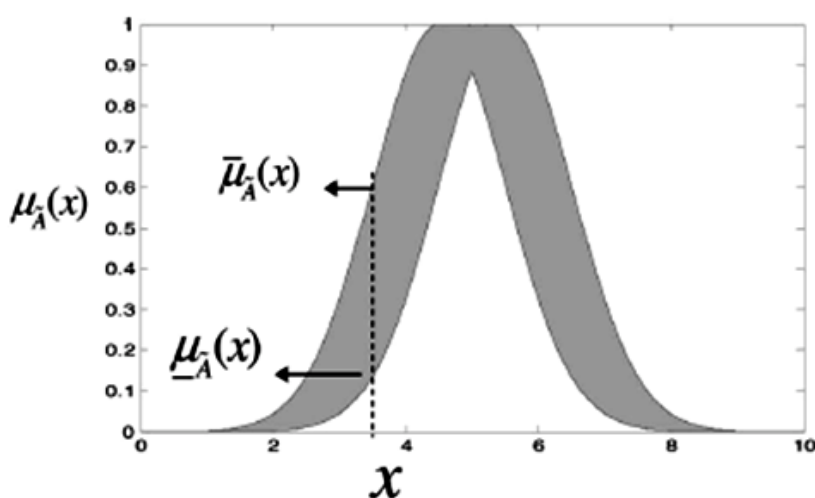

Figure 1. The mean uncertainty on a Gaussian membership.

A comprehensive review on the most successful application of T2 FLSs in classification and pattern recognition until 2011 has been done by Melin and Castillo [67]. Similarly, to the T1 FLS, a T2 FLS includes a fuzzifier, a rule base, fuzzy inference engine, and an output processor, as we can see in Figure 2 The output processor includes type-reducer and defuzzifier; it generates a T1 FSs output (from the type-reducer) or a number (from the defuzzifier) as described in detail by Karnik and Mendel [68–71].
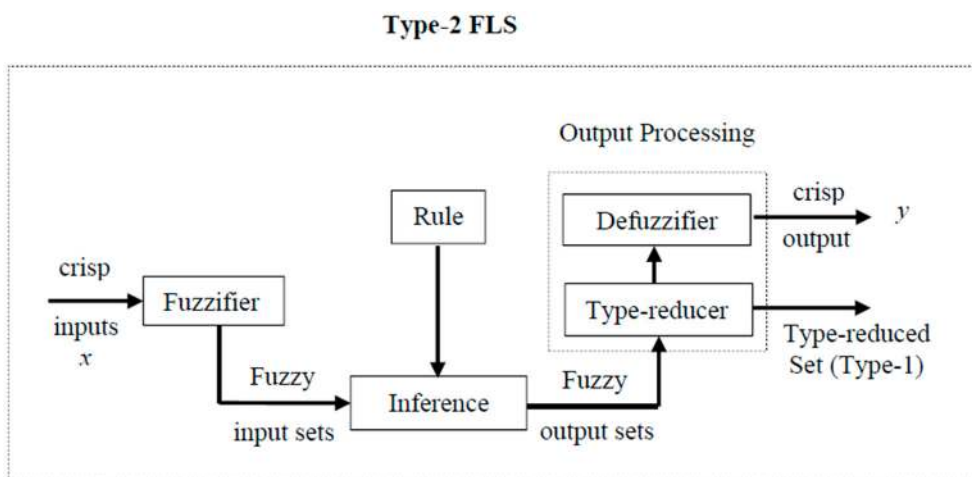

Figure 2. Basic structure of T2 fuzzy inference system.

4. Proposed Method

The proposed framework for road detection is shown in Figure 3. The proposed method is summarized in the steps following the figure.
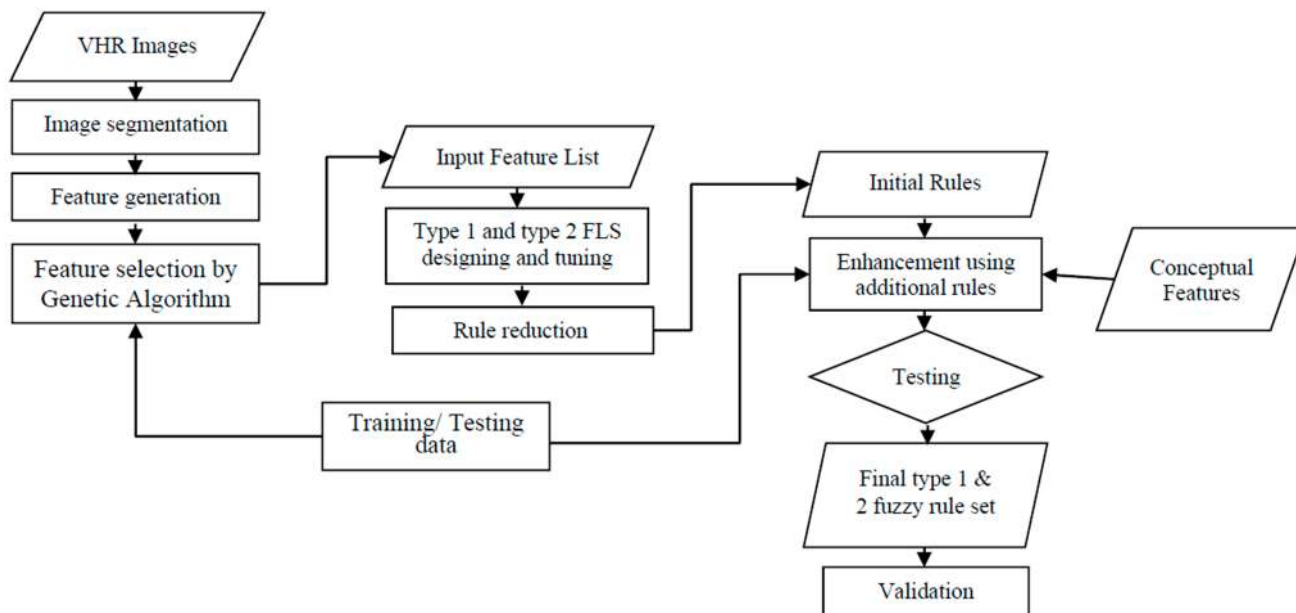
Figure 3. The proposed framework for road detection.

4.1. Object-Based Feature Generation

At first, the input data are to be prepared. Training data sets of satellite images containing a variety of objects such as vegetation, water, bare soil, buildings, parking lots and road objects are selected for rule generation. As the procedure is object oriented, image segmentation is initially performed for image object production. To overcome the shortcomings of pixel-based methods and also to reduce the semantic gap in image analysis, region-based algorithms have been developed [1–3]. Segmentation is a process in which the input image will be divided into homogeneous and separated regions. These homogeneous regions with similar indices, for example gray level, texture, shape, scale, *etc.*, are called image objects or image segments. Image segmentation is known as the preliminary stage of object-oriented algorithms. It groups some adjacent pixels as image objects and has the highest impact on the success of these algorithms. A considerable number of studies have compared object-based approaches to traditional pixel-based classification methods [25–29]. Moreover, many of these studies have indicated that object-based methods typically produce higher classification accuracies than pixel-based methods. In this paper, the multi-resolution segmentation, one of the most powerful segmentation algorithms proposed by Baatz and Schäpe for image segmentation and used in considerable literature [72–76], is selected for image segmentation. This approach extends regions so as to minimize image object heterogeneity. Object heterogeneity is determined by weighted color and shape parameters. Also, shape heterogeneity is calculated using compactness and smoothness criteria. The algorithm is described in detail in [1]. After image segmentation, different features can be generated from each object. The features can be categorized in four key groups: spectral, textural, shape, and combination features. In order to generalize the algorithm, the features are to be normalized. All image objects are

labeled as a road or non-road class. At this point, the data are prepared to be imported to the GA for optimum feature selection.

4.2. Feature Selection by the GA

As renowned search and optimization methods, GAs have been successfully applied to a wide range of image processing problems, such as image classification [77–79], image segmentation [80], feature extraction [81–83] and inverse modeling [84,85]. The GA is a technique that uses genetic evolution as a pattern for problem solving. In these algorithms, inputs and fitness functions should be defined according to the problem. The possible solutions are known as chromosomes, which consist of a number of genes that can take binary or continuous values. Evolution starts from a random set of all possible solutions, which is called the primary population. Then, fitness values can be calculated for the chromosomes based on the defined fitness function. In our optimization problem at this section, each chromosome is a $(1 \times n)$ binary vector in which n is the number of all features generated in the previous step. The digit "1" in each chromosome vector denotes that the corresponding feature affects the classification outcome and vice versa. From there, the next generation is produced based on the calculated fitness values using selection, crossover, and mutation operators. The chromosomes with higher fitness values have a higher chance to be selected in the next generation production and vice versa. Details about GAs can be found in [86]. To find best features in road detection, the chromosome solution using KNN algorithm is applied which is very simple, popular and highly efficient for pattern recognition. KNN algorithms have been used since 1970 in many applications including data mining, statistical estimation, and pattern recognition classification [87–89]. The KNN algorithm contains two main steps: first, find k training instances that are closest to the unknown instance; then, select the most commonly occurring classification for these k instances. After image classification, the fitness function should be designed for each chromosome solution based on the desired object classification. In this work, the kappa coefficient measurement is chosen as the fitness function computed from the confusion or error matrix [90]. Kappa is known as pessimistic accuracy measure. This property of kappa enables it to distinguish two FLS with little difference in classification result. For a completely accurate classification, the kappa coefficient would be 1. After KNN classification for each chromosome, the kappa coefficient is calculated. The GA procedure is repeated for the improvement of fitness values in consecutive generations until a stop criterion is met, such as a fixed number of generations, the highest ranking solution's fitness, population convergence, and so on.

4.3. Designing and Tuning the FLSs

The main structure of T2 FLS was described in Section 2. To realize the full potential of the optimum features, the space produced by the features will be divided into grids. Due to the extensive calculation performed by the T2 FLS, each feature space will be divided by three Gaussian membership functions using the Mamdani inference method for the consequent part, as previously illustrated. Besides, the Karnik-Mendel (KM) type reducer will be used for the precise output of the T2 FLS [70]. Mamdani fuzzy inference method is the most commonly seen fuzzy methodology that has been successfully applied in fields such as data classification, decision analysis, expert systems, and

computer vision. For additional evaluation, a T1 FLS that has exactly the same structure as a T2 FLS will be designed and tuned. The FLS parameter optimization procedure is explained in what follows.

Due to the large search space of T2 FLSs, we proposed an optimization method for FLS that is a hybrid GA consisting of a CCL approach and also containing a Pittsburgh approach. Within cooperative co-evolution, a solution for the problem to be solved is created through the unification of several individuals (sub-solution) that evolve into different populations, while within the competitive approach, a candidate sub-solution is evaluated based upon the results that it obtains after a set of competitions with several other sub-solutions. The CCL approach has been selected because of its ability to search and to efficiently find good fuzzy rules, and the Pittsburgh approach is selected to avoid trapping in local optimal solution because of the dependency of the chromosomes in the competitive stage. The details of proposed hybrid GA are explained as follows.

4.3.1. Initial Population Production

As previously mentioned, a hybrid GA consisting of Pittsburgh and CCL (P-CCL) is proposed for tuning the T2 FLS. The initialization step assigns the population values before the evolution process begins. At the first N, FLS parameters will be assigned. N denotes the total number of chromosomes in each generation. Because the population will be evolved through two independent procedures, the initial population must be coded according to the aforementioned coding method: P-CCL. In a Pittsburgh coding scheme, a single solution is responsible for the overall performance, with a fitness value assigned to that solution according to its performance. The coding scheme is concerned with the corresponding parameters of all of the membership functions of all features and consequent parts of all fuzzy rules that represent a full solution. In other words, the coding scheme exactly represents a T2 FLS, as depicted in Figure 4. In our Pittsburgh coding, "n" represents the number of optimum features that are the output of the GA-KNN strategy, as described in the previous section. Moreover, "*r*" denotes the number of rules in our FLS. m_1, m_2 and σ represent the uncertainty boundaries of the mean and variance of each membership function, respectively. With regard to the input data, the variance of each feature is considered to be a crisp number. $\underline{y}$ and $\bar{y}$ represent the upper and lower consequent values, respectively. It should be noted that "*i*" and "*n*" respectively indicate the *i*th membership function of each feature and number of the feature.
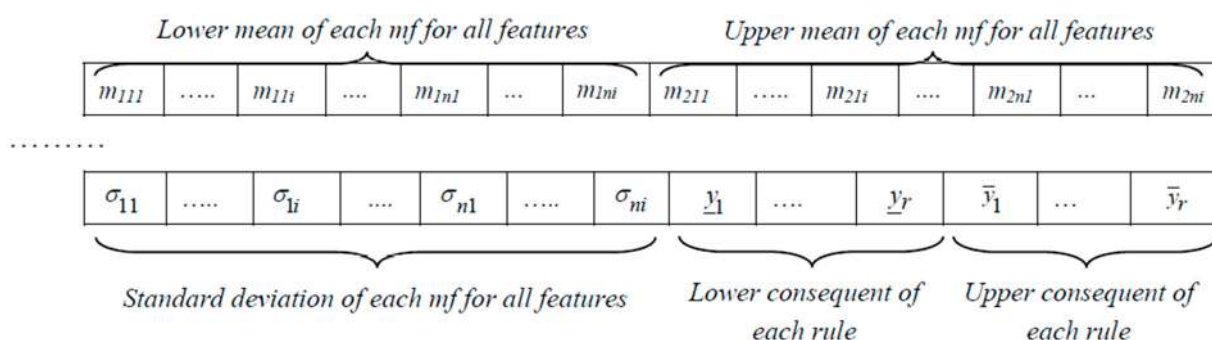

Figure 4. The scheme of the Pittsburg evolution coding of a T2 FLS.

The CCL evolution assumes that each sub-solution in a population represents only a partial solution to a problem. The goal of each sub-solution is to form a partial solution that can be combined with

other partial solutions in the current population to build an effective full solution. The structure of a scheme in the CCL evolution is shown in Figure 5. The coded scheme of a sub-solution is concerned with the corresponding parameters of membership functions and consequent part of a fuzzy rule that exactly represents a Mamdani fuzzy rule (a sub-solution) as plotted by Figure 6.
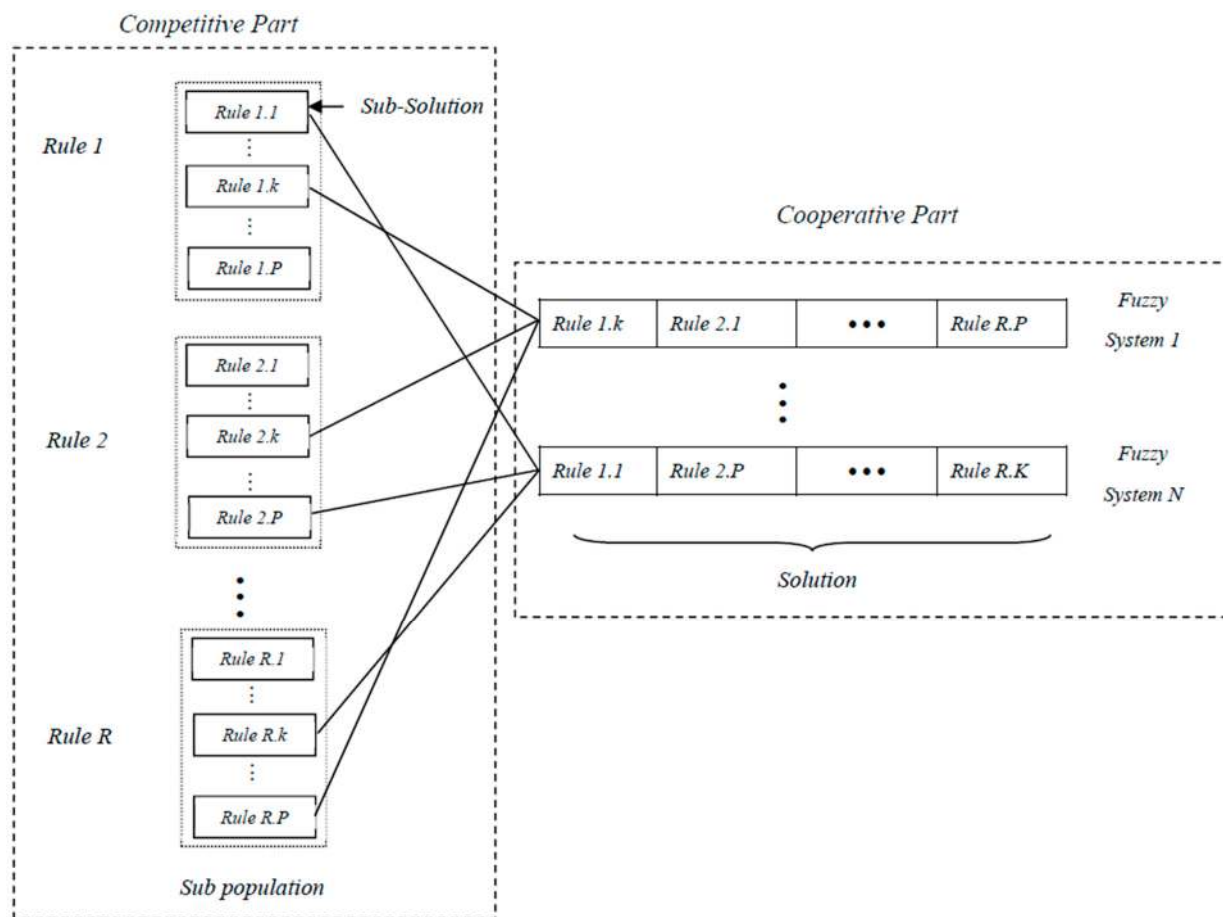
Figure 5. Scheme coding of a FLS through the CCL.
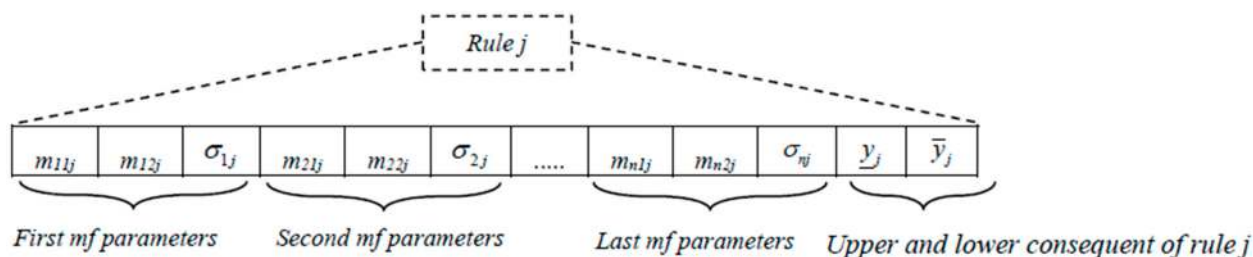
Figure 6. Scheme coding of a sub-solution in the proposed T2 FLS CCL.

4.3.2. Fitness Function

In the Pittsburgh evolution procedure described previously, a single individual (a solution) is responsible for the overall performance. The kappa coefficient measurement is proposed, such as the GA-KNN fitness function that was described in the feature selection step.

The fitness value calculation for each sub-solution in the CCL procedure is described as follows:

Step 1: Each pair of input-output is imported to a sub-solution. The rule firing will be calculated (F_i).

Step 2: The rule output will be calculated via the KM method and will be named Y_{iK}, where k represents the system output and *i* denotes the *i*th input-output training pair.

Step 3: The convergence measurement of each Y_{iK} from the ideal output (Y_{iT}) is computed as the following: $C_i = Y_{iT}/Y_{iK}$ or $C_i = Y_{iT}/Y_{iK}$. Values less than 1 are accepted. High C values indicate high rule performance.

Step 4: Finally, the efficiency of each rule can be calculated for all of the input-output training pairs using the following equation, where "n" is the training pair number: $EF_i = \Sigma(C_i \times F_i)/n$.

4.3.3. Reproduction, Crossover and Mutation

In the reproduction step, chromosome strings are copied according to their fitness values by roulette wheel selection method, known as one of the most popular reproduction methods. Roulette wheel, developed by Holland [86], was selected to avoid trapping in the local maximum. For Pittsburgh evolution, reproduction will be performed using a traditional roulette wheel for each FLS. The reproduction procedure for CCL will be performed for each sub-population using roulette wheel selection so as to opt for good sub-solutions in each sub-population. In other words, each rule in the sub-population competes with other rules that are present in the next generation. A full solution will be formed after competition and the selected rules will cooperatively form a full solution; however, certain inconsistencies will be produced as a consequence of rule dependency. Therefore, to complete the cooperation step, the membership function parameters of the rules in a solution will be fixed randomly. Some new chromosomes are produced based on the crossover probability of two selected chromosomes. In our proposed framework, this operator selects multi-combination points randomly for each pair, then the chromosomes combine and produce a new chromosome pair. The mutation operator randomly alters each gene with a small probability that is responsible for reintroducing lost gene values. Additionally, due to the long string for each chromosome, the mutation operator also enters a few new chromosomes. Along with the reproduction step, to complete the cooperative step in CCL evolution, inconsistent parameters will be fixed. The process of reproduction, crossover, and mutation is repeated until the convergence criterion is met.

4.4. Rule Reduction

Some rules may have existed in FLS fire in executing a few training samples; therefore, they could not contribute to the learning procedure. Due to this problem, it is understood that the parameters of the rules with low mean firing values were not tuned or reliable for testing samples that fire these rules with high firing values. Therefore, after the termination of tuning, these rules would be recognized and deleted from the FLS. Thus, we had a tuned FLS for both T2 and T1 that could be tested and enhanced in the next step.

4.5. Testing and Enhancement

In the previous section, the proposed T1 and T2 FLS were tuned using the proposed P-CCL genetic algorithm for the training data set. The training data set consists of samples from road and non-road

classes. All of the remaining data from the training data set source would be considered a test data set. Because the features used in the T2 FLS are restricted due to the tuning limitation, new rules will be generated using explorations of additional optimum feature views and histograms and prior knowledge of road objects. Additionally, certain efficient conceptual features, such as adjacency features, can be defined after the initial classification and can significantly improve the road detection result, which cannot be defined in pixel-based algorithms. The rules are generated in the IF-THEN form; moreover, for further generalization, as described in the feature generation step, all of the features must be normalized. Finally, after establishing the additional rule set, the test data set will be classified and evaluated.

4.6. Validation

After establishing the final T2 FLS, it must be validated by a validation data set that provides no contribution to the tuning rules. Other images are prepared, such as in training/testing data set preparation; these images are classified by the proposed road detection procedure, and the results are evaluated. For further evaluation, our proposed method is compared to the best results of the T1 FLS for both the training/testing and the validation data sets.

5. Implementation and Analysis

5.1. Input Data

In this study, pan-sharpened multi-spectral IKONOS_2 images with a 1-m spatial resolution and 11-bit radiometric resolution were used. A statistics-based fusion, implemented in the PCI software, was used for image pan sharpening [91]. The input data were divided into known groups of training/testing and validation data sets. The training/testing data set was used to tune the FLSs. The images taken from Hobart in Australia (1857 × 1725 pixels) and Kish Island in Iran (2317 × 1901 pixels), shown in Figure 7a,c, were selected for the training/testing data set for their specific object class. The validation result is the most important part of each automated algorithm evaluation. Therefore, to demonstrate the efficiency of our proposed FLS, other IKONOS images taken from Hamadan (1, 2) (1812 × 1282 pixels), (1588 × 1228 pixels), Yazd (1470 × 1228 pixels), Shiraz (1784 × 1353 pixels) in Iran, shown in Figure 7b,d,e,f, were selected for validation analysis.

5.2. Object-Based Feature Selection

The first step of the proposed procedure is image segmentation, which serves to produce regions as meaningfully as possible. A meaningful segmentation precisely represents the boundary of the feature of interest (e.g., buildings, roads, trees). Because a road network cannot be segmented into one region, to use potential road features such as linearity, connectivity, and homogeneity as well as to avoid under- and over-segmentation problems, it is more advantageous to segment, to the greatest extent possible, road objects into long regions that are not mixed with other objects in a non-road class.

Figure 7. The IKONOS images: (**a**) Taken from Hobart in Australia; (**b**) Taken from Hamedan in Iran; (**c**) Taken from Kish Island in Iran; (**d**) Taken from Yazd in Iran; (**e**) Taken from Hamedan in Iran; (**f**) Taken from Shiraz in Iran.

As mentioned previously, the segmentation algorithm proposed by Baatz and Schäpe [1] implemented in eCognition packages is used by knowledge engineers for this step. The segmentation parameters were set to 43, 0.5, and 0.3 for the scale parameter, shape, and compactness weight, respectively by trial-and-error. The segmentation result of the training data set is shown in Figure 8.
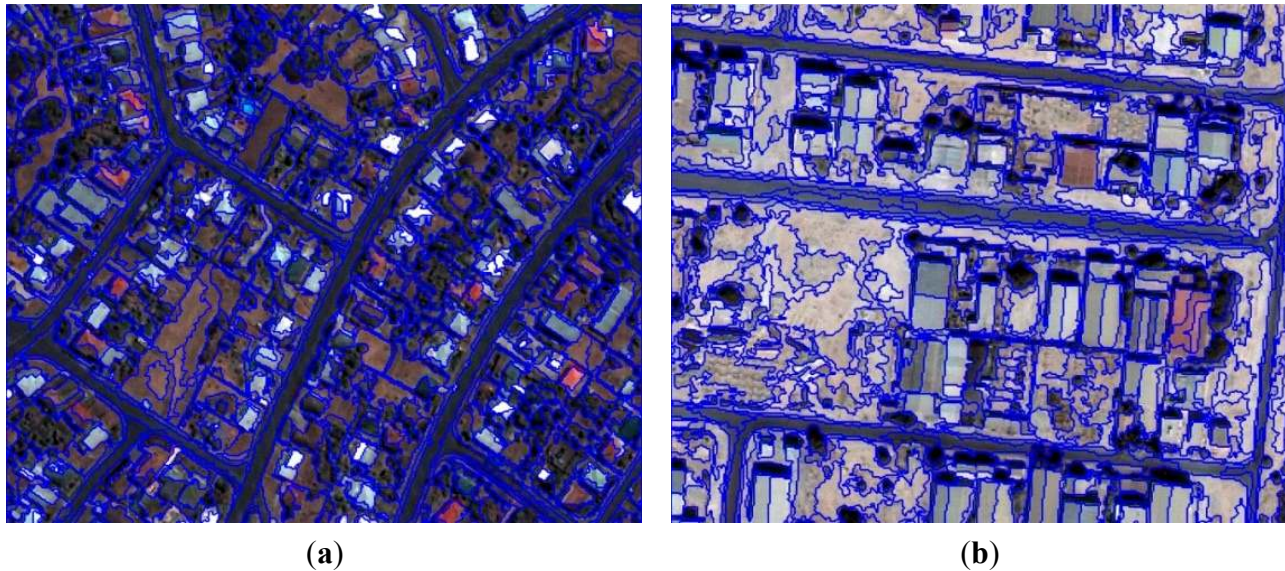

(a)   **(b)**

Figure 8. A segmented view of: **(a)** Hobart; **(b)** Kish.

After image segmentation, all of the features in Table 1 were generated for each image object, and they were imported into the GA-KNN algorithm.

Table 1. All of the features that should be generated for each object.

Spectral	Shape	Texture	Combination
Mean (for 4 bands:NIR,Red,Green,Blue)	Area	GLCM homogeneity (for 4 bands in all.dir)	Intensity/Density
Brightness	Asymmetry	GLCM contrast (for 4 bands in all.dir)	Saturation/Density
Max. diff	Shape index	GLCM dissimilarity (for 4 bands in all.dir)	Intensity/compactness
Standard deviation (for 4 bands)	Roundness	GLCM entropy (for 4 bands in all.dir)	Saturation/shape Index
Ratio (for 4 bands)	Rectangular fit	GLCM mean (for 4 bands in all.dir)	Intensity/Shape Index
Contrast to neighbor (for 4 bands)	width	GLCM stddev (for 4 bands in all.dir)	Area × Max diff/ Border length
Std. deviation to neighbor (for 4 bands)	Border index	GLCM ang. 2nd moment (for 4 bands in all.dir)	Ratio Red/Density
Mean diff. to neighbors (for 4 bands)	length		Area × Ratio red/Border length
Mean diff. to darker neighbors (for 4 bands)	Density		Hue/Density
Mean diff. to brighter neighbors (for 4 bands)	Elliptic fit		Hue/Shape Index
Hue	Compactness		Max diff/Density
Intensity	Length/Width		Max diff/Rectangular Fit
saturation	Border length		Max diff/Shape Index
NDVI			Ratio Red/Rectangular Fit
NDWI			Ratio Red/Shape Index

The initial population size of the GA algorithm was set to 600 due to the existence of approximately 60 genes for each chromosome. Empirically, the crossover and mutation rates were set to 0.66 and 0.05, respectively. One-hundred road objects and 100 non-road objects were selected as training

samples. In addition, 200 road and 200 non-road objects were selected as test samples for computing the kappa coefficient for each chromosome in the GA-KNN. The population convergence criterion was selected for evolution termination. This criterion terminates the evolution when the population is deemed to have converged. Experiments revealed five or seven nearest neighbors with the same features as the optimum ones. For a comprehensive evaluation of the best GA-KNN result, all of the remaining objects containing road and non-road objects were regarded as test data and added to the previous test data set. The optimum features identified by the GA-KNN strategy are shown in Table 2.

Table 2. Optimum features found by GA-KNN.

NDVI	Standard deviation Blue	Hue	Brightness
NDWI	GLCM Homogeneity Blue	Ratio Red	Saturation/Density

Description of the optimum features are summarized in the following in Table 3.

Table 3. Optimum Feature description.

	Feature Description
Brightness	Sum of the mean values of the layers containing spectral information divided by their quantity computed for an image object.
Standard deviation	Calculated from the layer values of all n pixels forming an image object.
Hue	The hue value of the HSI color space representing the gradation of color.
Saturation	The saturation value of the HSI color space representing the intensity of a specific hue. Relative purity of color; pure spectrum colors are fully saturated.
Ratio	The ratio of layer k reflects the amount that layer k contributes to the total brightness.
GLCM Homogeneity	It is a measure of the amount of local homogeneity in the image object.
NDVI	$(NIR - \mathrm{Re}d)/(NIR + \mathrm{Re}d)$
NDWI	$(Green - NIR)/(Green + NIR)$
Density	The density expressed by the area covered by the image object divided by its radius.

Due to the advantages of the object-based algorithm, certain structural features, such as area and length/width, as well as certain conceptual features, such as borders relative to neighboring objects and the mean difference to the neighbors that are definable after a primary classification, were added to the GA-KNN optimum features. Independently using these features may affect the road detection result; however, combining them with other features can be very helpful, such as human interpretation in road detection. Thus, the aforementioned features were added to the GA-KNN optimum features, and they were used in the generation of additional enhancement rules.

5.3. Type 2 FLS Designing and Tuning

As described in the previous step, eight features were identified by GA as optimum features in road detection from IKONOS images. Due to the large number of T2 FLS parameters, calculations and hardware limitations, all of the optimum features cannot be used in designing T2 FLS. Experiments show that our hardware systems allow for the use of a maximum of four features by selecting three Gaussian membership functions for each feature. Results of the constrained GA-KNN by maximum four features show that the standard deviation blue, hue, ratio red, saturation/density feature set has

greater accuracy than another foursome set. Decreasing the number of membership functions to two results in reduced accuracy, and increasing the number results in an increase in the search space and complexity. Designing a full T2 FLS that covers the entire features space with three membership functions for four features produces 81 rules. For each T2 membership function, two mean parameters and one variance parameter are considered, as shown in Figure 1. Experiments show that considering the uncertainty in the variance has no effect on the system quality. Regarding the Mamdani inference system, two parameters for T2 and one parameter for T1 FLS should be considered for each consequent. Therefore, 198 and 105 parameters must be solved for each T2 FLS and T1 FLS tuning, respectively, which is coded in the Pittsburgh scheme, as shown in Figure 5; moreover, 11 and 7 parameters must be solved for each rule as a sub-solution in a CCL scheme, as shown in Figure 5. Eighty percent of each generation will be allocated to the Pittsburgh strategy evolution, and owning to the rules correlation, 20% of each generation will be allocated to the CCL evolution algorithm. The initial population size of the random FLS parameters was set to 1000. Empirically, the Pittsburgh crossover, total chromosomes mutation and genes mutation were set to 0.62, 0.003 and 0.04, respectively. The CCL evolution reproduction rate and mutation rate received the respective values of 0.5 and 0.05. Because the main purpose of CCL evolution was to serve as an efficient tool for finding the best rules in each generation, the reproduction rate was set higher than it ordinarily is. The termination condition was set to 3000 generations, which was selected on account of system memory considerations. The data from 600 normalized road and non-road objects equally taken from Kish and Hobart IKONOS images were imported into the optimization algorithm as the training data set. These two images were chosen to improve the algorithm generalization. As previously mentioned, the kappa coefficient measurement was selected for each FLS, both T1 and T2. After the FLS optimization, the rules with firing values less than 0.01 were removed from the system. The optimized membership functions for both T1 and T2 FLSs are shown in Figure 9. In Figure 9 "mf$i$" denotes ith membership function of each feature. It appears that the T2 membership functions were generated by blurring the T1 membership functions, whereas, in reality, the results were yielded by the hybrid GA. Table 4 shows the accuracy results of the tuned T1 and T2 FLSs. The final results of the training step as presented in Table 4 show no significant differences between the two tuned FLSs for training data set. Where: Completeness = TP/(TP + FN) and Correctness= TP/(TP + FP) [92,93].

Table 4. Tuned FLSs accuracy evaluation for the training data set.

Accuracy	T2 FLS		T1 FLS	
	Road	**Non Road**	**Road**	**Non Road**
Completeness	0.97	0.9733	0.97	0.9667
correctness	0.9479	0.9848	0.9357	0.9848
Kappa	0.9379		0.9282	
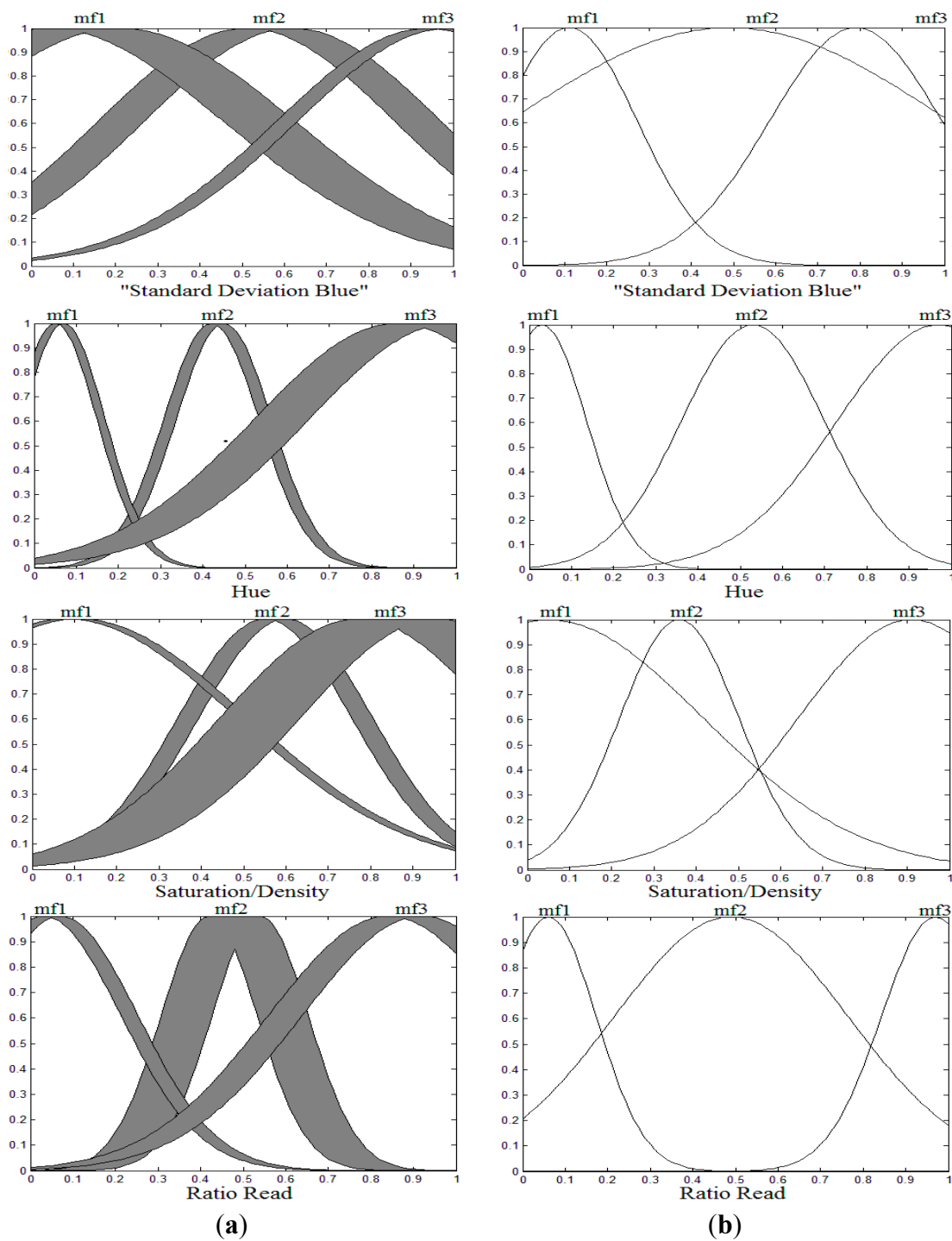
Figure 9. Final optimized membership function for input features: (**a**) T2 optimized membership function; (**b**) T1 optimized membership function; standard deviation blue, hue, saturation/density and ratio red respectively in the row.

5.4. Testing and Enhancement

At this step, the testing data set must be evaluated using the optimized T2 and T1 FLSs. on account of (Hobart and Kish images). The results of the testing data evaluation are presented in Table 5.

Table 5. Tuned FLSs accuracy evaluation for testing data set.

Class	Test Images	T2 FLS			T1 FLS		
		Completeness	Correctness	Kappa	Completeness	Correctness	Kappa
Road	Kish	0.8577	0.7926	0.8173	0.8587	0.7526	0.7946
	Hobart	0.8897	0.8036	0.8323	0.8852	0.7773	0.8141
Non Road	Kish	0.9920	0.9949	0.8173	0.9899	0.9949	0.7946
	Hobart	0.9839	0.9918	0.8323	0.9812	0.9914	0.8141

The results show that for the training and testing data set, the T1 and T2 FLS have good potential in training and have very similar performance in optimization. As previously described, some new rules could be generated by exploring the training/testing data with additional optimum feature views, histograms and prior knowledge of the road objects. Additionally, certain efficient conceptual features could be defined after the initial classification could significantly improve the road detection result.

Using prior knowledge and the exploration of the training/testing data sets, most of the vegetated cover and water object noises could be removed using the Normalized Difference Vegetation Index (NDVI) and the Normalized Difference Water Index (NDWI). Therefore, the basic rules generated based on these two known indices were as follows [94,95]: where T_i indicates ith threshold,

(1) If NDVI > T_1, then the class is non-road (vegetation).
(2) If NDWI > T_2, then the class is non-road (water object).

For more effective use of the NDVI index potentials and to reduce the probability of missing road objects with trees as neighbors, combining a linear-shaped feature with the mentioned index is suggested. Because an object with a high length/width value is indicated as an elongated object, the length/width feature combined with the NDVI is suggested for potential road objects, as outlined by the following rule:

(3) If T_3 < NDVI < T_1 and if length/width > T_4, then the class can be road.

As is the case with human interpretation, roads can be recognized as homogeneous objects. Thus, a rule using the homogeneity blue can be generated and added to the rule set:

(4) If homogeneity blue < T_5, then the class is non-road.

For further improvement, conceptual features, such as adjacency and connectivity, combined with structural features are proposed for removing non-road objects. Considering the connectivity of the road network, each road object must be connected to at least one other. Due to certain noises, such as shadows, pedestrian lines and bridges, combination of the linearity feature with the connectivity condition can be very helpful in removing non-road objects, as expressed by the following rule:

(5) If object length/width < T_4 and the border relative to the road objects = T_6, then the object is non-road.

To eliminate the noise ensued from cars and shadows, the following two simple rules were designed:

(6) If area < T_7 (m^2) and the border relative to the road objects > T_8, then the object is road (detecting cars on the road surface).

(7) If the area < T_9 (m^2) and the border relative to the road objects > T_{10}, and brightness < T_{11}, then the object is road (detecting shadows near the road surface).

As the final rule for detecting missed road objects, a combination of homogeneity, adjacency, similarity and linearity is introduced:

(8) If homogeneity blue > T_5 and $-T_{12}$ < mean difference in red to the neighbor road objects $<_+ T_{12}$ and length/width > T_4, then the object is road.

Using the training/testing data sets, the generated rules were revised and completed. The final parameters for the new rules are listed in the following:

T_1, T_{11} = 0.1, T_2 = 0.25, T_3, T_6 = 0, T_4 = 5, T_5 = 0.14, T_7 = 30, T_8, T_{10} = 0.6, T_9 = 50, T_{12} = 0.03.

The final road detection result on the Hobart and Kish IKONOS images using the proposed framework for T1 and T2 FLSs results and their human extracted reference images are shown in Table 6 and Figure 10, respectively. Figure 10a,b show the referenced detected road from the Hobart and Kish IKONOS images. Additionally, Figure 10c,d show our proposed T2 FLS road detection result after enhancement for the Hobart and Kish IKONOS images. It should be noted that all roads in the suburban area and road wider than ten meters in the urban area would be considered in the reference data. By comparing Tables 5 and 6, one can deduce that the rules added to T1 and T2 FLSs have improved the road detection results from testing data up to three percent. Besides, as observed in the Kish evaluation result, the missed road in T1 is better than the T2 FLS. It should be mentioned that due to their higher parameters, T2 FLSs are more probable to be trapped at local optimum points than T1 FLSs, given the computing systems at hand and their associated processing limitations.

(a)   (b)

Figure 10. *Cont.*

(c)   **(d)**

Figure 10. Training and testing evaluation: (**a,b**) The referenced road data of Hobart and Kish IKONOS image; (**c**,**d**) The final result of proposed road detection method from Hobart and Kish IKONOS image.

Table 6. Final evaluation of Hobart and Kish image.

Class	Test Images	T2 FLS			T1 FLS		
		Completeness	Correctness	Kappa	Completeness	Correctness	Kappa
Road	Kish	0.8615	0.8433	0.8454	0.8635	0.8081	0.8273
	Hobart	0.8933	0.8455	0.8581	0.8897	0.8272	0.8457
Non Road	Kish	0.9943	0.9950	0.8454	0.9927	0.9951	0.8273
	Hobart	0.9879	0.9921	0.8581	0.9862	0.9918	0.8457

5.5. Validation

In this section, the most important part of our proposed framework for road detection from IKONOS images that shows its high potential and efficiency in road detection is discussed. As explained in the previous sections, a T2 FLS using the Kish and Hobart IKONOS data set are tuned through a hybrid genetic strategy (P-CCL). Because the source of the training and testing data set is the same, only the accuracy assessment of testing data set is not sufficient and it sounds necessary for the generalization and validation assessment to evaluate our framework with some data sets having no contribution in the procedure established for road detection. The IKONOS images taken from Hamadan (1), yazd, Hamadan (2) and Shiraz and Yazd in Iran are used for the framework validation. They are, respectively, shown in Figure 7b,d,e,f. Figure 11 demonstrates portions of the image that were segmented using the segmentation parameters introduced in the previous section. The segmentation result of the validation set shows that the segmentation parameters for road detection have provided satisfactorily acceptable and desirable results; where the roads were segmented as elongated and homogeneous regions without over- or under-segmentation problems.
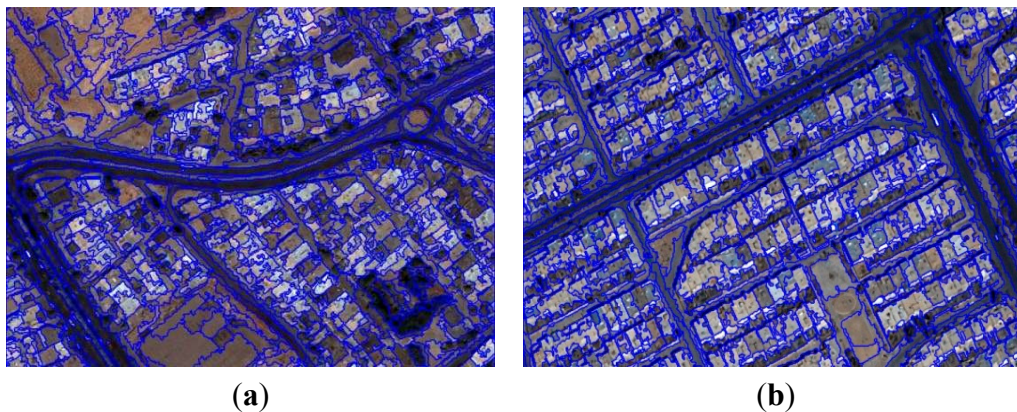
Figure 11. A segmented view of: (**a**) Shiraz image; (**b**) Yazd image.

After the segmentation step, as described in the previous step, the desired features were extracted from each image object and imported to the proposed algorithm. Table 7 shows the road detection validation results of the T2 FLS, the efficiency of which will be testified via classification of the validation data set by use of the T1 FLS established in the previous section, similar to our method. Figures 12a,b and 13a,b show the referenced road data from Shiraz, Yazd and Hamadan 1, 2 respectively. Based on the obtained results, the T1 FLS for the Shiraz and Yazd cases detects number of non-road objects as road objects and results in lower correctness accuracy. Also in the Hamadan 1, 2 data sets, the missed road objects by T1 FLS are considerable and lead to lower completeness accuracy. The proposed T2 FLS, as seen in Table 7, produces steadier results compared to those of T1 FLS.

Table 7. Validation results of optimized T1 and T2 FLSs.

Class	Validation Images	T2 FLS			T1 FLS		
		Completeness	Correctness	Kappa	Completeness	Correctness	Kappa
Road	Shiraz	0.8012	0.6961	0.7201	0.7840	0.5420	0.6018
	Yazd	0.8433	0.6675	0.7138	0.8307	0.4863	0.5589
	Hamadan1	0.7354	0.6801	0.6780	0.6561	0.6589	0.6255
	Hamadan2	0.8084	0.6464	0.6922	0.7218	0.5736	0.6056
Non Road	Shiraz	0.9683	0.9817	0.7201	0.9400	0.9796	0.6018
	Yazd	0.9543	0.9825	0.7138	0.9046	0.9801	0.5589
	Hamadan1	0.9676	0.9750	0.6780	0.9682	0.9678	0.6255
	Hamadan2	0.9634	0.9838	0.6922	0.9556	0.9765	0.6056

Table 8 as well as Figures 12 and 13 show the road detection validation results of T1 and T2 FLS after enhancement by the rule set for the four mentioned IKONOS Images. Figures 12c,d and 13c,d show the results of the framework for Shiraz, Yazd and Hamadan 1,2 IKONOS images, respectively. Also, Figures 12e,f and 13e,f show the final results of the T1 FLS method for the respective IKONOS images of Shiraz, Yazd and Hamadan 1,2.

Figure 12. (**a**,**b**) The referenced road data of Shiraz and Yazd IKONOS images. (**c**,**d**) The final result of proposed T2 FLS after enhancement. (**e**,**f**) The final result of T1 FLS after enhancement.

Figure 13. (**a,b**) The referenced road data of Hamadan 1,2 IKONOS images. (**c,d**) The final result of the proposed T2 FLS after enhancement. (**e**,**f**) The final result of T1 FLS after enhancement.

Table 8. Validation result of T1 and T2 FLSs after enhancement.

Class	Validation images	T2 FLS			T1 FLS		
		Completeness	Correctness	Kappa	Completeness	Correctness	Kappa
Road	Shiraz	0.8034	0.7455	0.7520	0.7883	0.6167	0.6604
	Yazd	0.8559	0.7043	0.7453	0.8357	0.5309	0.6015
	Hamadan1	0.7406	0.7021	0.6939	0.6587	0.6870	0.6426
	Hamadan2	0.8192	0.6813	0.7206	0.7326	0.6307	0.6490
Non Road	Shiraz	0.9751	0.9821	0.7520	0.9556	0.9803	0.6604
	Yazd	0.9609	0.9840	0.7453	0.9197	0.9810	0.6015
	Hamadan1	0.9706	0.9756	0.6939	0.9719	0.9682	0.6426
	Hamadan2	0.9683	0.9848	0.7206	0.9645	0.9776	0.6490

Comparing Tables 7 and 8 shows that the rule set has more effect on the T1 FLS and the correctness accuracy has been improved up to ten percent. Also, the proposed rule set recuperates the T2 FLS up to five percent. As observed in the validation images, the selected data are placed in dense urban areas and the validation results prove the high performance of our proposed method in road detection.

Although these results did not completely match the referenced road data ideally and had some misses and noise, they can be improved by some morphological operations or by the use of a gap detection algorithm in the road centerline extraction step, neither of which is the aim of this research. The training and testing evaluations show no important differences between T2 and T1 FLS. Additionally, it should be noted that T1 FLS tuning is much easier than for T2 FLS due to lower calculation times and optimization parameters (nearly half of T2 FLS parameters); therefore, the probability of falling into a local optimum point is less than that of T2 FLS using the available calculation systems. However, the validation results of T1 FLS are not comparable to our proposed framework. This is one remarkable point for our method. The evaluations show the T1 FLS is very sensitive to the training data set, and T2 evaluations demonstrate its high potential for handling uncertainty in the validation data set.

6. Conclusions

In this research, a new framework was proposed using T2 FS theory in combination with object-based image analysis to establish a generalized road detection framework from IKONOS images independent of training knowledge. In the field of image processing, we usually encounter many uncertainties, such as those caused by projecting a 3D object into a 2D image, uncertain boundaries, nonhomogeneous regions, poor and non-uniform lighting conditions and non-linearity of the imaging system. An interesting alternative is to employ T2 FSs, which augment fuzzy models with expressive power to develop models, which efficiently capture the factor of uncertainty. A classic GA scheme is offered to find the most effective features in the road detection procedure and a hybrid GA consisting of Pittsburgh and cooperative-competitive learning strategies is proposed and designed for T2 FLS parameter optimization. After fixing the T2 FLS parameters, to improve the accuracy, some conceptual features were added to the FSs in if-then rule format utilizing prior knowledge and the training data set. The Kish and Hobart case study shows the high potential of our proposed procedure in T2 FS tuning. The most prominent achievement of our research was seen in the validation

evaluation, which shows how successful the proposed framework is for road detection in independent IKONOS satellite images. The achievement of 79%, 68% and 70% averaged completeness, correctness and kappa accuracies using the optimized T2 FLS, as well the achievement of 80%, 72% and 72.5% averaged completeness, correctness and kappa accuracies using the proposed T2 FLS framework after enhancement for independent images, demonstrates the capability and efficiency of the method in automatically identifying road objects. For more validation, a T1 FLS with the same structure as T2 is tuned. Evaluations show that T1 FLS performance in training is very close to the proposed T2 FLS framework, but the generalization and validation assessment demonstrate lower accuracy with significant differences from the proposed T2 FLS. Due to the large calculation time and extensive computations of T2 FLS, using a parallel processor may be very helpful to extend and improve the proposed method. Although the results did not completely match the referenced road data ideally and had some misses and noise, they can be improved using some morphological operations or by means of a gap detection algorithm in the road centerline extraction step.

Acknowledgments

Author Contributions

Maryam Nikfar and Mohammad Javad Valadan Zoej developed the concept and designed the research. Maryam Nikfar performed the research including preparing and analyzing the data. Mohammad Javad Valadan Zoej was primary supervisor and leaded the research work. Mehdi Mokhtarzadeh and Mahdi Aliyari Shoorehdeli were the first and the second co-supervisor of this work respectively. Mohammad Javad Valadan Zoej, Mehdi Mokhtarzadeh and Mahdi Aliyari Shoorehdeli provided expert knowledge about methods, and participated in the discussions, editing and revisions of the paper. All authors discussed the results and implications and commented on the manuscript at all stages.

Conflicts of Interest

The authors declare no conflict of interest.

References

1. Baatz, M.; Schäpe, A. Multiresolution segmentation: An optimization approach for high quality multi-scale image segmentation. In *Angewandte Geographische Informationsverarbeitung XII*; Strobl, J., Blaschke, T., Eds.; Wichmann-Verlag: Heidelberg, Germany, 2000; pp. 12–23.
2. Herold, M.; Scepan, J.; Muller, A.; Gunter, S. Object-oriented mapping and analysis of urban landuse/cover using IKONOS data. In Proceedings of the 22nd EARSEL Symposium Geoinformation for European-Wide Integration, Prague, Czech Republic, 4–6 June 2002; pp. 531–538.
3. Benz, U.; Hofmann, P.; Willhauck, G.; Lingenfelder, I.; Heynen, M. Multiresolution object-oriented fuzzy analysis of remote sensing data for GIS-ready information. *ISPRS J. Photogramm. Remote Sens.* **2004**, *58*, 239–258.

4. Mendel, J.M.; John, R.B. T2 fuzzy sets made simple. *IEEE Trans. Fuzzy Syst.* **2002**, *10*, 117–127.

5. Mena, J.B. State of the art on automatic road extraction for GIS update: A novel classification. *Pattern Recognit. Lett.* **2003**, *24*, 3037–3058.

6. Laptev, I.; Mayer, H.; Lindeberg, T.; Eckstein, W.; Steger, C.; Baumgartner, A. Automatic extraction of roads from aerial images based on scale-space and snakes. *Mach. Vis. Appl.* **2003**, *12*, 13–23.

7. Gruen, A.; Li, H. Semi-automatic linear feature extraction by dynamic programming and LSB snakes. *Photogramm. Eng. Remote Sens.* **1997**, *63*, 985–995.

8. Doucette, P.; Agouris, P.; Stefanidis, A. Automated road extraction from high resolution multispectral imagery. *Photogramm. Eng. Remote Sens.* **2004**, *70*, 1405–1416.

9. Zhang, Q.; Couloigner, I. Wavelet approach to road extraction from high spatial resolution remotely sensed imagery. *Geomatica* **2004**, *58*, 33–39.

10. Mokhtarzade, M.; Valadan Zoej, M.J. Road detection from high-resolution satellite images using artificial neural networks. *Int. J. Appl. Earth Obs. Geoinf.* **2007**, *9*, 32–40.

11. Peng, T. Incorporating generic and specific prior knowledge in a multiscale phase field model for road extraction from VHR Images. *IEEE J. Sel. Top. Appl. Earth Obs. Remote Sens.* **2008**, *1*, 130–148.

12. Valero, S.; Chanussot, J.; Benediktsson, J.A.; Talbot, H.; Waske, B. Advanced directional mathematical morphology for the detection of the road network in very high resolution remote sensing images. *Pattern Recognit. Lett.* **2010**, *31*, 1120–1127.

13. Movaghati, S.; Moghaddamjoo, A.; Tavakoli, A. Road extraction from satellite images using particle filtering and extended kalman filtering. *IEEE Trans. Geosci. Remote Sens.* **2010**, *48*, 2807–2815.

14. Mirnalinee, T.T.; Das, S.; Varghese, K. An integrated multistage framework for automatic road extraction from high resolution satellite imagery. *J. Indian Soc. Remote Sens.* **2011**, *39*, 1–25.

15. Shao, Y. Application of a fast linear feature detector to road extraction from remotely sensed imagery. *IEEE J. Sel. Top. Appl. Earth Obs. Remote Sens.* **2011**, *4*, 626–631.

16. Shi, W.; Miao. Z.; Debayle, J. An integrated method for urban main-road centerline extraction from optical remotely sensed imagery. *IEEE Trans. Geosci. Remote Sens.* **2014**, *52*, 3359–3372.

17. Miao, Z.; Wang, B.; Shi. B.; Wu, H. A method for accurate road centerline extraction from a classified image. *IEEE J. Sel. Top. Appl. Earth Obs. Remote Sens.* **2014**, *7*, 4762–4771.

18. Boyko. A; Funkhouser, T. Extracting roads from dense point clouds in large scale urban environment. *ISPRS J. Photogramm. Remote Sens.* **2011**, *66*, s2–s12.

19. Yu, Y.; Li, J.; Guan, H.; Jia, F.; Wang, C. Learning hierarchical features for automated extraction of road markings from 3-D mobile LIDAR point clouds. *IEEE J. Sel. Top. Appl. Earth Obs. Remote Sens.* **2015**, *8*, 709–726.

20. He, C.; Yang, F.; Yin, S.; Deng, X.; Liao, M. Stereoscopic road network extraction by decision-level fusion of optical and SAR imagery. *IEEE J. Sel. Top. Appl. Earth Obs. Remote Sens.* **2013**, *6*, 2221–2228.

21. Lu, P.; Du, K.; Yu, W.; Wang, R.; Deng, Y.; Balz, T. A new region growing-based method for road network extraction and its application on different resolution SAR images. *IEEE J. Sel. Top. Appl. Earth Obs. Remote Sens.* **2014**, *7*, 4772–4783.

22. Blaschke, T.; Strobl, J. What's wrong with pixels? Some recent developments interfacing remote sensing and GIS. *GeoBIT/GIS.* **2001**, *6*. 12–17.

23. Cleve, C.; Kelly, M.; Kearns, F.R.; Moritz, M. Classification of the wild land urban interface: A comparison of pixel- and object-based classifications using high resolution aerial photography. *Comput. Environ. Urban Syst.* **2008**, *32*, 317–326.

24. Blaschke, T. Object based image analysis for remote sensing. *ISPRS J. Photogramm. Remote Sens.* **2010**, *65*, 2–16.

25. Baltasavias, E. Object extraction and revision by image analysis using existing geo data and knowledge: Current status and steps towards operational systems. *ISPRS J. Photogramm. Remote Sens.* **2004**, *58*, 129–151.

26. Laliberte, A.S.; Rango, A.; Havstad, K.M.; Paris, J.F.; Beck, R.F.; McNeely, R.; Gonzalez, A.L. Object-oriented image analysis for mapping shrub encroachment from 1937 to 2003 in southern New Mexico. *Remote Sens. Environ.* **2004**, *93*, 198–210.

27. Frohn, R.C.; Hinkel, K.M.; Eisner, W.R. Satellite remote sensing classification of thaw lakes and drained thaw lake basins on the North Slope of Alaska. *Remote Sens. Environ.* **2005**, *97*, 116–126.

28. Ehlers, M.; Gähler, M.; Janowsky, R. Automated techniques for environmental monitoring and change analyses for ultra-high-resolution remote sensing data. *Photogramm. Eng. Remote Sens.* **2006**, *72*, 835–844.

29. Im, J.; Jensen, J.R.; Tullis, J.A. Object-based change detection using correlation image analysis and image segmentation. *Int. J. Remote Sens.* **2008**, *29*, 399–423.

30. Huang, X.; Zhang, L. An SVM ensemble approach combining spectral, structural, and semantic features for the classification of high-resolution remotely sensed imagery. *IEEE Trans. Geosci. Remote Sens.* **2013**, *51*, 257–272.

31. Huang, X.; Zhang, L. Road centreline extraction from high-resolution imagery based on multiscale structural features and support vector machines. *Int. J. Remote Sens.* **2009**, *30*, 1977–1987.

32. Zarrinpanjeh, N.; Samadzadegan, F.; Schenk, T. A new ant based distributed framework for urban road map updating from high resolution satellite imagery. *Comput. Geosci.* **2013**, *54*, 337–350.

33. Grote, A.; Heipke, C.; Rottensteiner, F. Road network extraction in suburban areas. *Photogramm. Rec.* **2012**, *27*, 8–28.

34. Agouris, P.; Gyftakis, S.; Stefanidis, A. Using a fuzzy supervisor for object extraction within an integrated geospatial environment. *Int. Arch. Photogramm. Remote Sens. Spat. Inf. Sci.* **1998**, *32*, 191–195.

35. Amini, J.; Lucas, C.; Saradjian, M.R.; Azizi, A.; Sadeghian, S. Fuzzy logic system for road identification using IKONOS images. *Photogramm. Rec.* **2002**, *17*, 493–503.

36. Hinz, S.; Wiedemann, C. Increasing efficiency of road extraction by self-diagnosis. *Photogramm. Eng. Remote Sens.* **2004**, *70*, 1457–1466.

37. Bacher, U.; Mayer, H. Automatic road extraction from multispectral high resolution satellite images. *Int. Arch. Photogramm. Remote Sens. Spat. Inf. Sci.* **2005**, *36*, Part 3/W24, 29–34.

38. Mayer, H.; Hinz, S.; Bacher, U.; Baltsavias, E. A test of automatic road extraction approaches. *Int. Arch. Photogramm. Remote Sens. Spat. Inf. Sci.* **2006**, *36*, 209–214.

39. Mohammadzadeh, A.; Tavakoli, A.; Valadan Zoej, M.J. Road extraction based on fuzzy logic and mathematical morphology from pan-sharpened IKONOS images. *Photogramm. Rec.* **2006**, *21*, 44–60.

40. Singh, P.P.; Garg, R.D. A two-stage framework for road extraction from high-resolution satellite images by using prominent features of impervious surfaces. *Int. J. Remote Sens.* **2014**, *35*, 8074–8107.

41. Melin, P.; Castillo, O. *Hybrid Intelligent Systems for Pattern Recognition Using Soft Computing*; Springer-Verlag: Berlin, Germany, 2005.

42. Cordón, O.; Herrera, F.; Hoffmann, F.; Magdalena, L. *Genetic Fuzzy Systems: Evolutionary Tuning and Learning of Fuzzy Knowledge Bases*; World Scientific: Singapore, 2001; Chapters 1–5, pp. 1–350.

43. Lopez, M.; Melin, P.; Castillo, O. Optimization of response integration with fuzzy logic in ensemble neural networks using genetic algorithms. *Stud. Comput. Intell.* **2008**, *154*, 129–150.

44. Sanchez, D.; Melin, P. Modular neural network with fuzzy integration and its optimization using genetic algorithms for human recognition based on iris, ear and voice biometrics. In *Soft Computing for Recognition Based on Biometrics*; Studies in Computational Intelligence; Springer: Berlin/Heidelberg, Germany, 2010; Volume 312, pp. 85–102.

45. Hidalgo, D.; Castillo, O.; Melin, P. T1 and T2 fuzzy inference systems as integration methods in modular neural networks for multimodal biometry and its optimization with genetic algorithms. *Inf. Sci.* **2009**, *179*, 2123–2145.

46. Wu, D.; Tan, W.W. Genetic learning and performance evaluation of interval T2 fuzzy logic controllers. *Eng. Appl. Artif. Intell.* **2006**, *19*, 829–841.

47. Cordón, O.; Gomide, F.; Herrera, F.; Hoffmann, F.; Magdalena, L. Ten years of genetic fuzzy systems: Current framework and new trend. *Fuzzy Sets Syst.* **2004**, *141*, 5–31.

48. Cordón, O. A historical review of evolutionary learning methods for Mamdani-type fuzzy rule-based systems: Designing interpretable genetic fuzzy systems. *Int. J. Approx. Reason.* **2011**, *52*, 894–913.

49. Castillo, O.; Melin, P. Optimization of T2 fuzzy systems based on bio-inspired methods: A concise review. *Inf. Sci.* **2012**, *205*, 1–19.

50. Papadakis, S.E.; Theocharis, J.B. A GA-based fuzzy modeling approach for generating TSK models. *Fuzzy Sets Syst.* **2002**, *131*, 121–152.

51. Casillas, J.; Martínez, P.; Benítez, A.D. Learning consistent, complete and compact sets of fuzzy rules in conjunctive normal form for regression problems. *Soft Comput.* **2009**, *13*, 451–465.

52. Sanza, J.; Fernández, A.; Bustince, H.; Herrerac, F. A genetic tuning to improve the performance of fuzzy rule-based classification systems with interval-valued fuzzy sets: Degree of ignorance and lateral position. *Int. J. Approx. Reason.* **2011**, *52*, 751–766.

53. Ishibuchi, H.; Nakashima, T.; Murata, T. Performance evaluation of fuzzy classifier systems for multidimensional pattern classification problems. *IEEE Trans. Syst. Man Cybern.* **1999**, *29*, 601–618.

54. Gonzblez, A.; Pérez, R. SLAVE: A genetic learning system based on an iterative approach. *IEEE Trans. Fuzzy Syst.* **1999**, *7*, 176–191.

55. González, A.; Herrera, F. Multi-stage genetic fuzzy systems based on the iterative rule learning approach. *Mathw. Soft Comput.* **1997**, *4*, 233–249.

56. Cordón, O.; Del Jesús, M.J.; Herrera, F.; Lozano, M. MOGUL: A methodology to obtain genetic fuzzy rule-based systems under the iterative rule learning approach. *Intell. Syst.* **1999**, *14*, 1123–1153.

57. Stavrakoudis, D.G.; Theocharis, J.B.; Zalidis, G.C. A multistage genetic fuzzy classifier for land cover classification from satellite imagery. *Soft Comput.* **2011**, *15*, 2355–2374.

58. Palacios, A.M.; Sánchez, L.; Couso, I. Extending a simple genetic cooperative-competitive learning fuzzy classifier to low quality datasets. *Evol. Intell.* **2009**, *2*, 73–84.

59. Dorronsoro, B.; Danoy, G.; Nebro, A.J.; Bouvry, P. Achieving super-linear performance in parallel multi-objective evolutionary algorithms by means of cooperative coevolution. *Comput. Oper. Res.* **2013**, *40*, 1552–1563.

60. Wang, X.; Cheng, H.; Huang, M. QoS multicast routing protocol oriented to cognitive network using competitive coevolutionary algorithm. *Expert Syst. Appl.* **2014**, *41*, 4513–4528.

61. Chandra, R.; Frean, M.; Zhang, M. Crossover-based local search in cooperative co-evolutionary feedforward neural networks. *Appl. Soft Comput.* **2012**, *12*, 2924–2932.

62. Pena-Reyes, C.A. Fuzzy CoCo: A cooperative-coevolutionary approach to fuzzy modeling. *IEEE Trans. Fuzzy Syst.* **2001**, *9*, 727–737.

63. Zadeh, L.A. Fuzzy logic and approximate reasoning. *Syntheses* **1975**, *30*, 407–428.

64. Mizumoto, M.; Tanaka, K. Some properties of fuzzy sets of type 2. *Inf. Control* **1976**, *31*, 312–340.

65. Mizumoto, M.; Tanaka, K. Fuzzy sets and their operations. *Inf. Control* **1981**, *48*, 30–48.

66. Castillo, O.; Melin, P. *T2 Fuzzy Logic: Theory and Applications*; Springer-Verlag: Berlin, Germany, 2008.

67. Melin, P.; Castillo, O. A review on the applications of T2 fuzzy logic in classification and pattern recognition. *Expert Syst. Appl.* **2013**, *40*, 5413–5423.

68. Karnik, N.N.; Mendel, J.M.; Liang, Q. T2 fuzzy logic systems. *IEEE Trans. Fuzzy Syst.* **1999**, *7*, 643–658.

69. Karnik, N.N.; Mendel, J.M. Operations on T2 fuzzy sets. *Fuzzy Sets Syst.* **2001**, *122*, 327–348.

70. Karnik, N.N.; Mendel, J.M. Centroid of a T2 fuzzy set. *Inf. Sci.* **2001**, *132*, 195–220.

71. Mendel, J. *Uncertain Rule-Based Fuzzy Logic Systems: Introduction and Directions*; University of Southern California: Los Angeles, CA, USA, 2000; Chapters 7–10, pp. 213–350.

72. Mallinis, G.; Koutsias, N.; Tsakiri-Strati, M.; Karteris, M. Object-based classification using Quickbird imagery for delineating forest vegetation polygons in a Mediterranean test site. *ISPRS J. Photogramm. Remote Sens.* **2008**, *63*, 237–250.

73. Dragut. L; Eisank, C. Automated object-based classification of topography from SRTM data. *Geomorphology* **2012**, *141–142*, 21–33.

74. Schneevoigt, N.J.; Linden, S.V.D.; Thamm, H.-P.; Schrott, L. Detecting alpine landforms from remotely sensed imagery: A pilot study in the Bavarian Alps. *Geomorphology* **2008**, *93*, 104–119.

75. Lucas, R.; Rowlands, A.; Brown, A.; Keyworth, S.; Bunting, P. Rule-based classification of multi-temporal satellite imagery for habitat and agricultural land cover mapping. *ISPRS J. Photogramm. Remote Sens.* **2007**, *62*, 165–185.

76. Gamanya, R.; Maeyer, P.D.; Dapper, M.D. An automated satellite image classification design using object-oriented segmentation algorithms: A move towards standardization. *Expert Syst. Appl.* **2007**, *32*, 616–624.

77. Stavrakoudis, D.G.; Theocharis, J.B.; Zalidis, G.C. A boosted genetic fuzzy classifier for land cover classification of remote sensing imagery. *ISPRS J. Photogramm. Remote Sens.* **2011**, *66*, 529–544.

78. Tseng, M.H.; Chen, S.J.; Hwang, G.H.; Shen, M.Y. A genetic algorithm rule-based approach for land-cover classification. *ISPRS J. Photogramm. Remote Sens.* **2008**, *63*, 202–212.

79. Wen, X.; Zhang, H.; Zhang, J.; Jiao, X.; Wang, L. Multiscale modeling for classification of SAR imagery using hybrid EM algorithm and genetic algorithm. *Prog. Nat. Sci.* **2009**, *19*, 1033–1036.

80. Nikfar, M.; Valadan Zoej, M.J.; Mohammadzadeh, A.; Mokhtarzade, M.; Navabi, A. Optimization of multiresolution segmentation by using a genetic algorithm. *J. Appl. Remote Sens.* **2012**, *6*, 1–18.

81. Li, S.; Wu, H.; Wan, A.; Zhu, J. An effective feature selection method for hyperspectral image classification based on genetic algorithm and support vector machine. *Knowl.-Based Syst.* **2011**, *24*, 40–48.

82. Puig, D.; Garcia, M.A. Automatic texture feature selection for image pixel classification. *Pattern Recognit.* **2009**, *39*, 1996–2009.

83. Krawiec, K.; Bhanu, B. Visual learning by coevolution feature synthesis. *IEEE Trans. Syst. Man Cybern.* **2005**, *35*, 409–425.

84. Chang, C.H.; Liu, C.C. Wen, C.G. Integrating semi analytical and genetic algorithms to retrieve the constituents of water bodies from remote sensing of ocean color. *Opt. Express* **2007**, *15*, 252–265.

85. Ines, A.V.; Honda, K. On quantifying agricultural and water management practices from low spatial resolution RS data using genetic algorithms: A numerical study for mixed-pixel environment. *Adv. Water Resour.* **2005**, *28*, 856–870.

86. Holland, J. *Adaptation in Natural and Artificial Systems*; University of Michigan Press: Oxford, UK, 1975; pp. 62–143.

87. Yu, C.; Cui, B.; Wang, S.; Su, J. Efficient index-based KNN join processing for high-dimensional data. *Inf. Softw. Technol.* **2007**, *49*, 332–334.

88. Chen, J.H. KNN based knowledge-sharing model for severe change order disputes in construction. *Autom. Constr.* **2008**, *17*, 773–779.

89. Saini, I.; Singh, D.; Khosla, A. QRS detection using *K*-Nearest Neighbor algorithm (KNN) and evaluation on standard ECG databases. *J. Adv. Res.* **2013**, *4*, 331–334.

90. Bishop, Y.M.M.; Fienberg, S.E.; Holland, P.W. *Discrete Multivariate Analysis: Theory and Practice*; MIT Press: Cambridge, MA, USA, 1975; pp. 105–171.

91. Zhang, Y. Understanding image fusion. *Photogramm. Eng. Remote Sens.* **2004**, *70*, 657–661.

92. Wiedemann, C.; Heipke, C.; Mayer, H.; Jamet, O. Empirical evaluation of automatically extracted road axes. In *Empirical Evaluation Methods in Computer Vision*; Bower, K.J., Philips, P.J., Eds.; IEEE Computer Society Press: Los Alamitos, CA, USA, 1998; pp. 172–187.

93. Yang, Y.; Lohmann, P.; Heipke, C. Genetic algorithms for the unsupervised classification of satellite images. *Int. Arch. Photogramm. Remote Sens. Spat. Inf. Sci.* **2006**, *36*, 179–184.

94. Hamedianfar, A.; Shafri, H.Z.M.; Mansor, S.; Ahmad, N. Improving detailed rule-based feature extraction of urban areas fromWorldView-2 image and LIDAR data. *Int. J. Remote Sens.* **2014**, *35*, 1876–1899.

95. Jin, X.; David, C.H. An integrated system for automatic road mapping from high-resolution multi-spectral satellite imagery by information fusion. *Inf. Fusion* **2005**, *6*, 257–273.